The processing aspects of the interferometric imaging spectrometer

(EE391 project report)
Ying-zong Huang
Joint work with Ulrich Barnhöfer and Sameer Bhalotra

1 Introduction

A natural scene contains not merely "colors" but spectral emissions that are not fully detectable by conventional imaging systems, such as a digital camera. The usual means to extract spectral information is with a hyperspectral imager, which filters light at different wavelengths and records their intensities. The interferometric imaging spectrometer (IIS) is an experimental device that extracts spectral information a different way, by generating and capturing light interference patterns.

The IIS embeds an interferometer within a conventional imaging system. Therefore, a key feature of the IIS is that it detects spectral information at all locations of a 2D scene in parallel. Coupled with per-pixel processing implementable using simple analog circuits, the IIS is capable of directly extracting from a scene specific spectral properties of interest – for example, the widths of spectral peaks. Detecting the width of spectral peaks has been the focal point of efforts with the IIS. We examine the processing steps necessary for that purpose and show experimental results and derived applications.

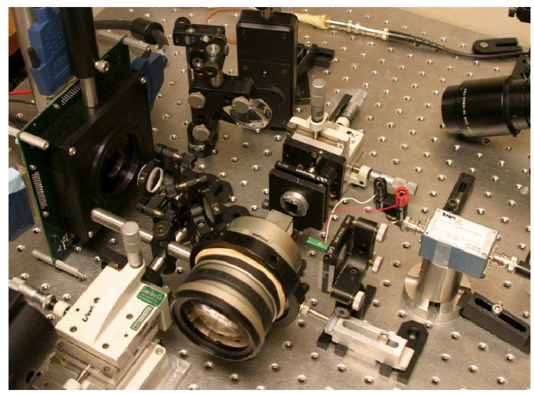

Figure 1: Interferometric imaging spectrometer.

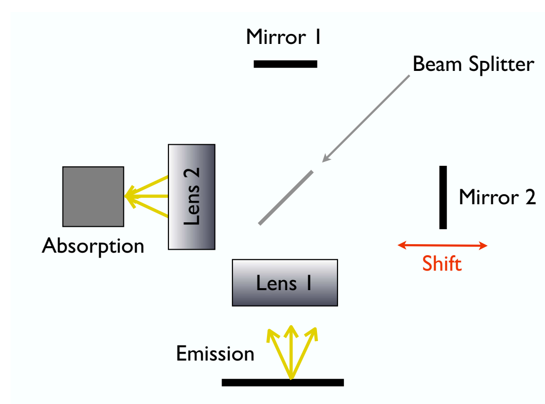

Figure 2: System schematic

2 System operation & analysis

The interferometric imaging spectrometer is shown in **Figure 1** and diagrammed in **Figure 2**. Light from each point in the scene enters an imaging lens (Lens 1) and is split into two paths by the Beam Splitter. One path is reflected at Mirror 1 and the other at Mirror 2. Mirror 1 is held fixed, while a piezoelectric device attached to Mirror 2 moves it in a periodic pattern along the optical axis. Light from the two paths is recombined at the Beam Splitter and is sent

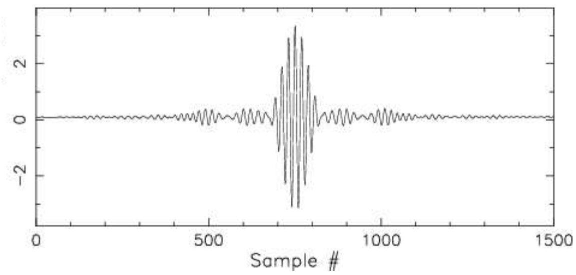

Figure 3: Example of an interferogram

through a final imaging lens (Lens 2) for detection by a high speed CMOS imager [1].

2.1 Interferometric pattern

When Mirror 2 is at the zero-point, where the optical path lengths of the two paths through the system are equal, then the image that forms at the CMOS imager is a conventional intensity image of the scene. If Mirror 2 is at any other point, an optical path length difference develops between the two paths through the system, and an interference image forms at the CMOS imager.

As Mirror 2 sweeps back and forth from one side of the zero-point to the other, the CMOS imager captures a set of images. The imager's capturing sequence is triggered by the driving waveform to the piezoelectric device attached to Mirror 2. At one end of the mirror motion, the imager is triggered and at the other end of the mirror motion, the imager ceases capturing. Each pixel on the imager thus captures an *interferogram* (**Figure 3**) and the imager as a whole captures a 2D interferogram, which is a sequence of images in time (**Figure 4**). The finite range of displacements scanned by Mirror 2 limits the spectral resolution of the system.

2.2 Spectral emission & interferogram [2, 4]

Given that the length of photons is many orders of magnitude longer than the maximum optical path length difference encountered in the IIS, we can treat, for the calculation of the interferograms, all photon wave functions as having infinite extent. We also assume that our image sensor is ideal in photon detection (flat frequency response and 100% quantum efficiency).

A photon of length L is represented by its wave function

$$\psi(z,t) = \frac{1}{\sqrt{L}} e^{ik(z-ct)}$$

where k is the wave number and c is the speed of light. A photon passing through the IIS where Mirror 2 is at displacement x with respect to the zero-point has the wave function (after a slight change in coordinates):

$$\begin{aligned}
\psi(z,t) &= \frac{1}{2\sqrt{L}} \{ e^{ik[(z-x)-ct]} + e^{ik[(z+x)-ct]} \} \\
&= \frac{1}{2\sqrt{L}} e^{ik(z-ct)} (e^{ikx} + e^{-ikx}) \\
&= \frac{1}{\sqrt{L}} e^{ik(z-ct)} \cos(kx)
\end{aligned}$$

Thus, the probability of detection of this photon is

$$\begin{aligned}
|\psi(z,t)|^2 &= \frac{\cos^2(kx)}{L} \int_{-\frac{L}{2}}^{\frac{L}{2}} \left| e^{2ik(z-ct)} \right|^2 dz \\
&= \cos^2(kx) \\
&= \cos^2(2\pi\bar{\nu}x)
\end{aligned}$$

A point of emission has a spectrum defined by the average photon flux spectral density function $s(\bar{\nu})$, $\bar{\nu} \in [0, \infty)$. If instead the spectrum is given in $\sigma(\lambda)$, we can convert it by the equivalence $s(\bar{\nu}) = \lambda^2\sigma(\lambda) = \bar{\nu}^{-2}\sigma(\bar{\nu}^{-1})$. Also define the modified spectrum $\hat{s}(\bar{\nu}) = \frac{1}{2}[s(\bar{\nu}) + s(-\bar{\nu})]$. Then the expected photon flux at Mirror 2 displacement x is

$$\begin{aligned}
\phi(x) &= \int_0^\infty s(\bar{\nu}) \, |\psi(z,t)|^2 \, d\bar{\nu} \\
&= \int_0^\infty s(\bar{\nu}) \cos^2(2\pi\bar{\nu}x) d\bar{\nu} \\
&= \int_0^\infty s(\bar{\nu}) [\frac{1}{2} + \frac{1}{2}\cos(4\pi\bar{\nu}x)] d\bar{\nu} \\
&= \frac{1}{2}\int_0^\infty s(\bar{\nu}) d\bar{\nu} + \frac{1}{2}\int_{-\infty}^\infty \hat{s}(\bar{\nu}) e^{i4\pi\bar{\nu}x} d\bar{\nu} \\
&= \frac{1}{2}\Phi + \frac{1}{2}\int_{-\infty}^\infty \hat{s}(\bar{\nu}) e^{i2\pi\bar{\nu}(2x)} d\bar{\nu} \\
&= \frac{1}{2}\Phi + \frac{1}{2}\mathfrak{F}^{-1}\{\hat{s}(\bar{\nu})\}(2x) \\
&= \frac{1}{2}\Phi + \frac{1}{2}\mathfrak{F}\{\hat{s}(\bar{\nu})\}(2x)
\end{aligned}$$

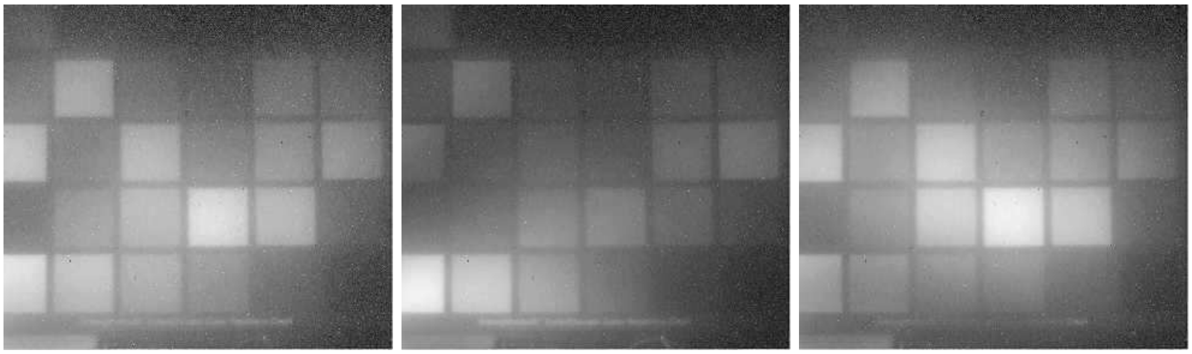

Figure 4: A few frames from a 2D interferogram

Clearly, $\phi(x)\Delta t$, where Δt is the integration time on the imager, is the interferogram for that point. The last line above establishes that the basic relationship between the emission spectrum of a point ($\bar{\nu}$-domain) and its interferogram (x-domain) is the Fourier transform.

Specifically, since $\hat{s}(\bar{\nu})$ is a real and even function, $\phi(x)$ is also real and even. The first term of $\phi(x)$ is equal to half the total photon flux Φ at the point, whereas the second term is half the Fourier transform of the modified spectrum $\hat{s}(\bar{\nu})$, evaluated at the optical path difference $2x$.

2.3 Peak width & coherence

From the interferogram decomposition expression for $\phi(x)$, we see that each peak in $\bar{\nu}$-domain corresponds roughly to, in the x-domain, the sum of (1) an offset of the conventional intensity generated by the peak; and (2) a cosine at the center frequency modulated by an enveloped that is the Fourier transform of the peak shape. Therefore, a narrowband peak results in a slowly decaying sinusoidally varying interferogram and a wideband peak results in a quickly decaying sinusoidally varying interferogram. By linearity, multiple peaks (or multiple light sources) in the $\bar{\nu}$-domain will also see their interferograms summed in the x-domain. The amount by which the interferogram envelope persists away from the zero-point is a quantity termed coherence.

2.4 Different peak widths

Figure 5 shows details of three sources. On the left are their emission spectra (of the $\sigma(\lambda)$ type). On the right are interferograms simulated using the expressions derived here. The three sources have different peak widths and the interferograms have different envelope structure.

2.5 Different peak frequencies

Figure 6 shows three LEDs of different center wavelengths. With substantially the same peak widths, their interferograms have the same envelope structure, which is invariant to shifts in center frequency.

3 Coherence detection

Distinguishing between narrowband peaks and wideband peaks in spectra is one way to detect certain types of sources. By measuring coherence, we obtain a measure of the selectivity of the dominant peak in the spectrum. The simple relationship between peak width and coherence means that low complexity methods to detect peak widths using the IIS are realizable.

Several circuit-implementable processing methods to detect coherence were developed. We describe a particularly straightforward version.

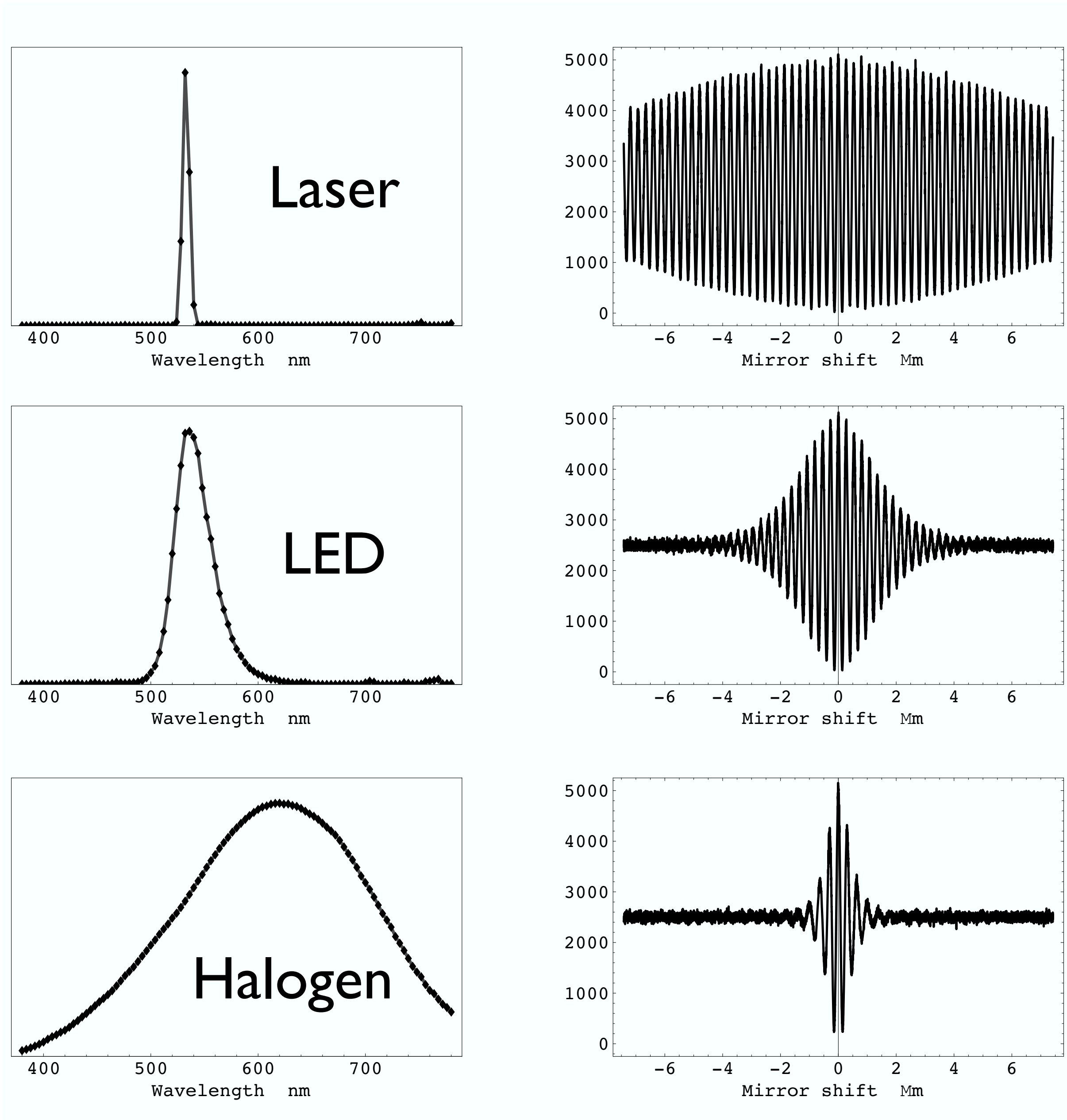

Figure 5: Spectra and interferograms of three source types

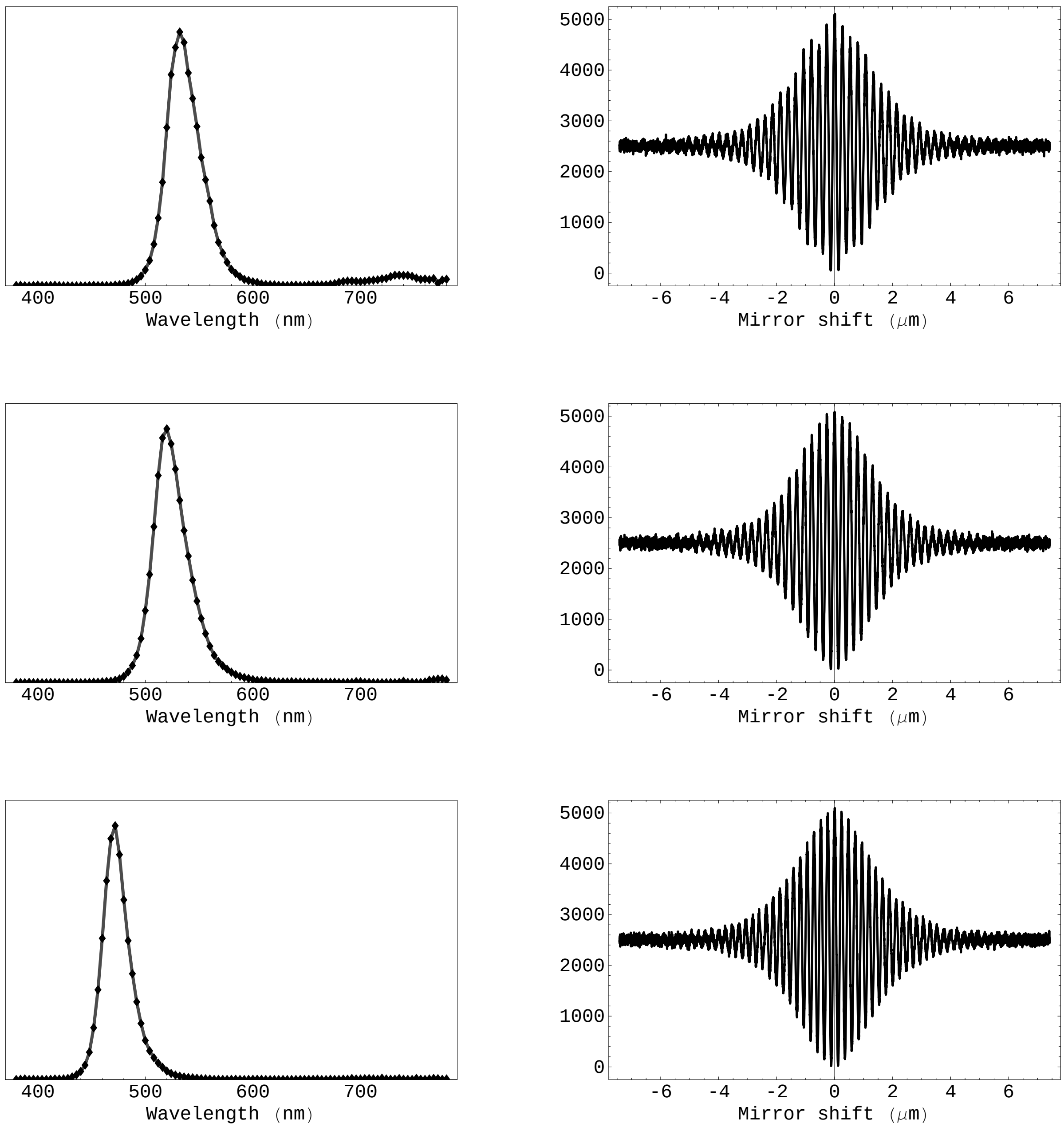

Figure 6: Spectra and interferograms of three LEDs. From top to bottom: GaP green LED, InGaN green LED, blue LED.

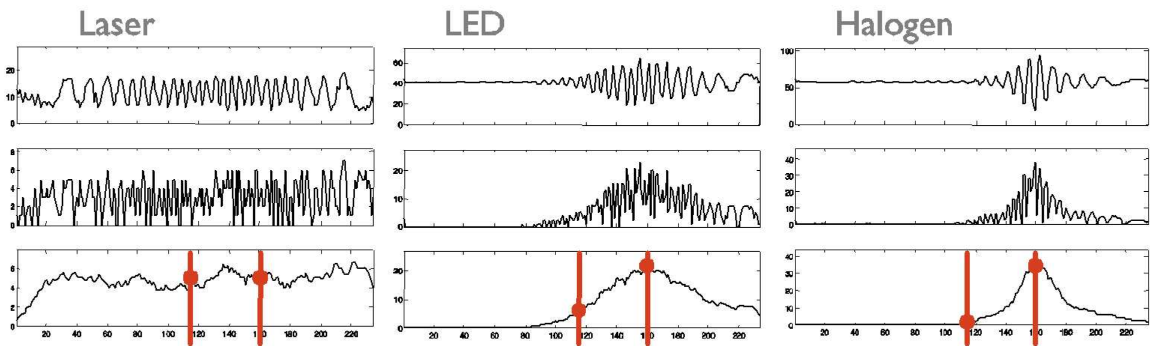

Figure 8: Demonstration of coherence detection. Each column displays information on one type of source. The top row shows interferograms measured from the IIS. The middle row shows the same after AC coupling and taking absolute value. The bottom row shows interferogram envelopes after low-pass filtering, with red bars indicating the locations of the selected zero-point and x_0.

Figure 7: Three light sources. From left to right: halogen, LED, laser.

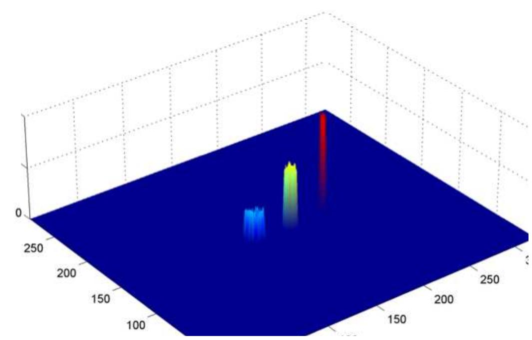

Figure 9: Coherence measure $\hat{\phi}(x_0)/\hat{\phi}(0)$.

First, if we are not interested in the center frequency of the light or its intensity, we can ignore the non-varying intensity offset and the sinusoidal frequency in the interferogram. To extract the envelope on the sinusoid, a standard AM demodulation circuit suffices to demodulate the interferogram at each pixel by AC coupling, taking the absolute value, and low-passing. Now, suppose for each pixel-wise interferogram of the 2D interferogram, $\hat{\phi}(x)$ denotes the envelope of the interferogram $\phi(x)$ thus obtained. We use $\frac{\hat{\phi}(x_0)}{\hat{\phi}(0)}$ as the coherence measure. The zero-point location is selected ahead of time by maximum detection on the interferogram envelopes from across the 2D interferogram; x_0 is at an appropriate offset from the zero-point, tunable to the envelope decay rates (hence spectra peak widths) of interest.

4 Experiments & applications

4.1 Three sources

Figure 7 is a scene with the same three sources shown in Figure 5. They differ in spectral peak widths. We demonstrate the ability to distinguish between them by coherence detection.

Figure 8 gives the measurements from the IIS taken at locations in the scene corresponding to the sources and the results of the pixel-wise processing

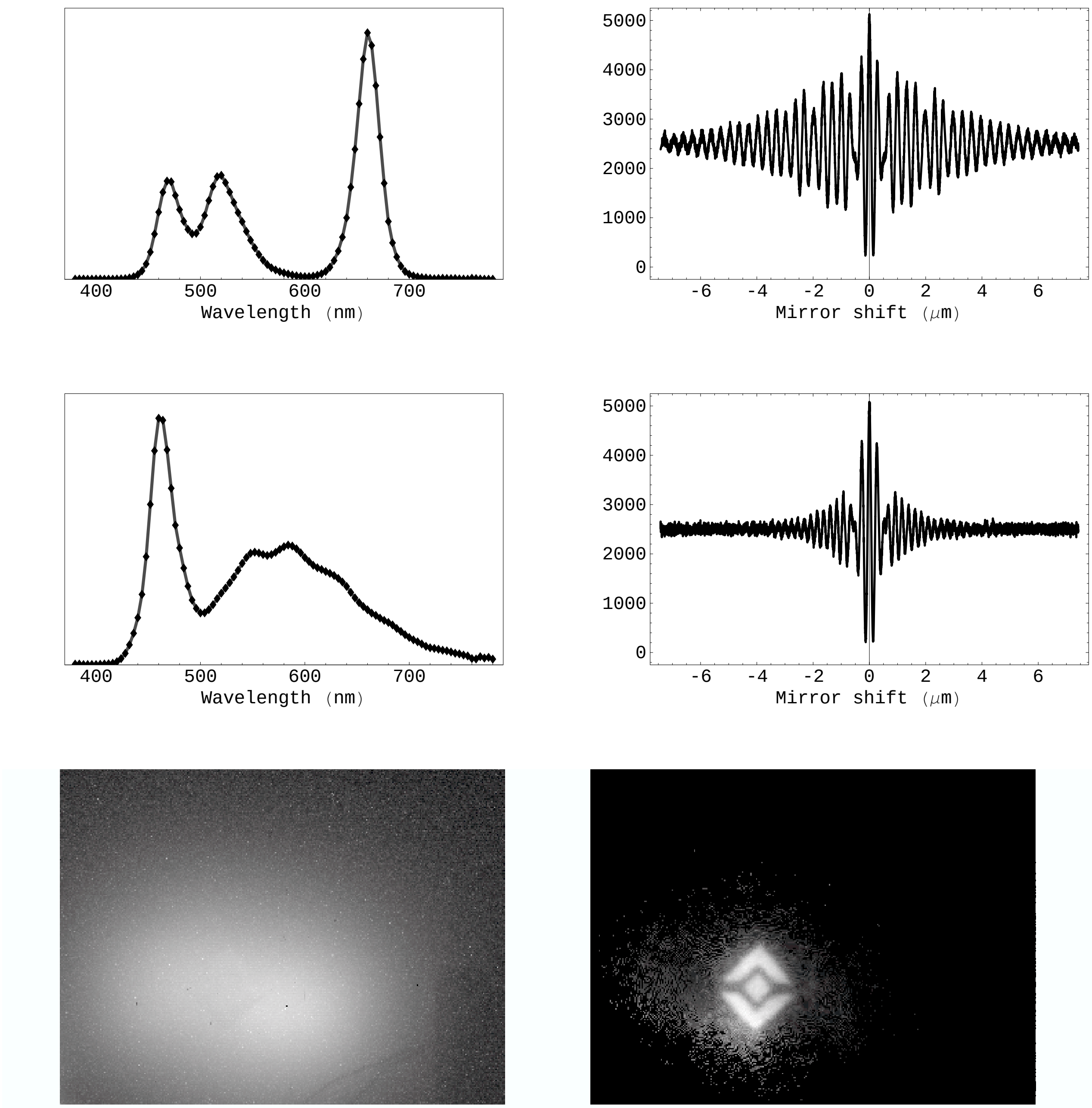

Figure 10: Hidden tag: a “barcode” surface emitting a narrowly peaked spectrum (top spectrum) is concealed in a surrounding surface that emits a broadband spectrum (middle spectrum). While the spectra emitted from the two Lambertian surfaces are different, both emit the same white color (same color coordinates) and the same intensity. Thus a conventional imager sees a homogenous surface (bottom left), while the IIS with coherence detection reveals the secret (bottom right), i.e. the “barcode.”

described in the previous section. A map of the processed coherence measure over the scene is given in **Figure 9**. Regardless of the original relative source intensities, the three sources are easily distinguishable.

4.2 Hidden tags

An important application of the IIS is invisible tagging. Specifically, coherence detection using the IIS can recover intentionally hidden spectral information not visible to a conventional imager (even a color one).

For example, a conventional imager is unable to distinguish between a broadband green light and a narrowband green LED. Indeed, in this case, the subtle spectral difference would be invisible even to the eye. We can take advantage of this by placing secret narrowband tags or beacons into natural broadband scenes. Only a 2D hyperspectral device, such as the IIS with coherence detection, can reveal the tags or beacons by specifically distinguishing them from the scene based on peak width differences. See **Figure 10**.

4.3 Hyperspectral imaging

By inverting the 2D interferogram measured using the IIS, we can recreate the full spectrum at each pixel. This allows us to generate a high dynamic range, hyperspectral 2D image (and possibly video) of the scene from a grayscale imager.

First, we remove skew in the experimental interferograms due to the nonlinear mirror motion at the endpoints of each sweep. Then, we remove the DC component of the interferogram (assumed to be $\frac{1}{2}\Phi$) and apply the Fourier transform, inverting the process for simulating interferograms based on spectra. The noisy and window-limited interferogram measurement puts a fundamental restriction on the resolution and accuracy of the recovered spectrum. However, we already obtain a good facsimile even without more sophisticated processing. **Figure 11** shows a scene rendered from recreated spectra and **Figure 12** shows the process for one pixel of the image.

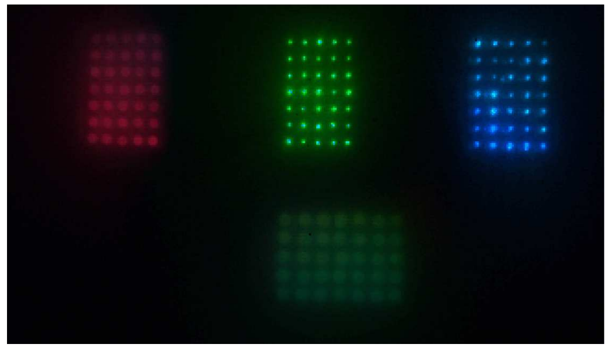

Figure 11: Scene of color (top) and white (bottom) LEDs rendered from a 2D interferogram captured on the IIS.

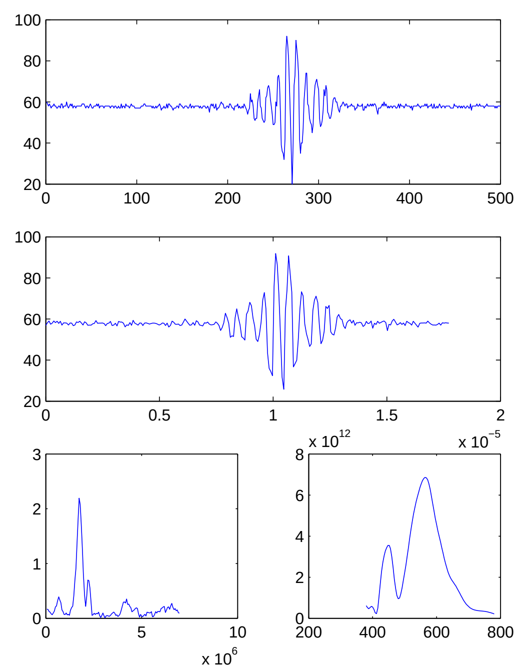

Figure 12: Inverting an interferogram. The raw captured interferogram (top) at a pixel on one of the white LEDs is compensated for skew due to mirror motion (middle) and inverted to obtain $s(\bar{\nu})$ (bottom left) and $\sigma(\lambda)$ (bottom right). The actual spectrum is the middle panel of Figure 10.

5 Conclusion

The interfermoetric imaging spectrometer combines the compact spectral acquisition capabilities of an interferometer with the 2D parallel operation of an image sensor array to form a 2D hyperspectral imager. The x-domain in which it operates and in which interferogram images are generated, is well suited for simple yet powerful processing methods to detect the spectral peak widths anywhere in a 2D scene using coherence detection. These methods also lend themselves well to feasible implementations. This enables a number of imaging scenarios and valuable applications such as the hidden tags.

Further work continues to characterize the system, including analyzing its noise properties and the exact effects of mirror motion on spectral resolution.

6 Acknowledgement

I would like to thank Ulrich Barnhöfer and Sameer Bhalotra for providing much guidance and for having built and troubleshooted a device sensitive to even small misalignment. As this is a joint work, many ideas described are attributable to them. I also thank Professor Miller for letting me sign up for EE391 to work on this.

References

[1] S. Kleinfelder, S. H. Lim, X. Q. Liu, and A. El Gamal, "A 10,000 frames/s CMOS digital pixel sensor," in *IEEE Journal of Solid State Circuits*, Vol. 36, No. 12, Pages 2049-2059 (2001).

[2] E. Hecht, *Optics*, Addison-Wesley, Reading, MA (1987).

[3] J. E. Chamberlain, *The principles of interferometric spectroscopy*, John Wiley & Sons, New York (1979).

[4] R. J. Bell, *Introductory Fourier transform spectroscopy*, Academic Press, New York (1972).